Radiation Physics and Chemistry 226 (2025) 112172

Contents lists available at ScienceDirect

Radiation Physics and Chemistry

journal homepage: www.elsevier.com/locate/radphyschem

Comprehensive remote calibration of detectors in a radiological surveillance network: From basic response to high-level data analysis

A. Cerezo [a,*], I. Reichardt [a], E. Prieto [a], R. Casanovas [a], C. Rovira [b], M. Salvadó [a]

[a] Unitat de Física Mèdica, Facultat de Medicina i Ciències de la Salut, Universitat Rovira i Virgili, Sant Llorenç 21, ES-43201, Reus, Tarragona, Spain
[b] Servei de Coordinació d'Activitats Radioactives, Departament d'Empresa i Treball, Generalitat de Catalunya, ES-08038, Barcelona, Spain

ARTICLE INFO

Handling editor: Chris Chantler

Keywords:
Remote calibration
Spectrometry
Detectors
Surveillance network
$LaBr_3(Ce)$
$SrI_2(Eu)$

ABSTRACT

We present a new procedure to remotely calibrate gamma spectrometry detectors installed in the open air used in surveillance networks. The procedure includes energy calibration, determination of the energy resolution and estimation of the activity concentration. Our Proportional ROI-Cleaning algorithm (Cerezo et al., 2023) has been applied to different detector types and dimensions ($LaBr_3(Ce)$, $SrI_2(Eu)$ and NaI(Tl)). These detectors are assembled in different measuring configurations (direct and with particulate filter). The usefulness of our method as a surveillance technique was confirmed by the detection of ^{75}Se, ^{131}I, ^{192}Ir and ^{60}Co in some locations of the Radiological Surveillance Network of Catalonia (Spain).

1. Introduction

The Euratom Treaty requires each Member State to stablish the necessary infrastructures to carry out real-time monitoring of the level of radioactivity in air, water and soil, ensuring the compliance of basic standards (Union, 2000). In Spain there is an environmental radiological surveillance network (Alegría et al., 2023; Ontalba et al., 2022; Sáez-Muñoz et al., 2024), as in other Member States (Abida et al., 2008; De Felice, 2001; Hiemstra et al., 2009; Kessler et al., 2018; Leontaris et al., 2018; Madruga, 2008; Neumaier, 2017; Stöhlker et al., 2019; Štuhec et al., 2006; Toivonen et al., 2008). The XVRAC (Xarxa de Vigilància Radiològica Ambiental de la Generalitat de Catalunya or Environmental Radiological Surveillance Network of Catalonia), the network installed in Catalonia (NE Spain), acquires data since 1986.

The nuclear incident marked as a 2 in the INES scale in Ascó nuclear power plant in 2007 (Consejo de Seguridad Nuclear, n.d.) was the starting point of the improvement of the Network. As explained in (Casanovas et al., 2011), this incident revealed that the information obtained with Geiger-Müllers and proportional detectors implemented in the Network was insufficient and it concluded that implementing high precision gamma spectrometry in real time would provide much more information (Dąbrowski et al., 2017). Since then, the Network has expanded to include scintillation detectors.

Currently, the real-time environmental radiological surveillance network consists of 35 monitors distributed around Catalonia as shown in Fig. 1: Twenty-four direct monitors without shielding with $1''\times1''$, $2''\times2''$ $LaBr_3(Ce)$, $3''\times3''$ NaI(Tl) and $2''\times2''$ $SrI_2(Eu)$ implemented detectors; ten monitors for aerosol surveillance using a particulate filter (RARM-F) (Casanovas et al., 2014a)with $2''\times2''$ $LaBr_3(Ce)$ and $SrI_2(Eu)$ detectors; two monitors with direct measurement using two shielded detectors (RARM-D2) (Casanovas et al., 2014b), where NaI(Tl) or $LaBr_3(Ce)$ detectors are used; and, finally, two NaI(Tl) water monitors (Casanovas et al., 2013) for the surveillance of the water from Ebre River.

Each one of these 35 monitors generate, every 10 min, an accumulated gamma spectrum that is sent for further analysis. This means that, per year, the Medical Physics Unit analyses more than a million of raw spectra. Clearly, the large volume of data makes it impossible to manually analyse each one of the spectra. For that reason, in recent years, our group has developed and improved several algorithms and methodologies to stabilize, analyse the data, and derive values of activity concentration and ambient dose equivalent H*(10) in real time (Casanovas et al., 2012a, 2016; Cerezo et al., 2023; Prieto et al., 2018a).

One of the most tedious steps in the network maintenance is performing the energy and resolution calibration of each station regularly. It requires to visit each one of the monitor locations with radioactive calibration sources. For that reason, our group has developed a new methodology to perform these calibrations remotely, eliminating the

* Corresponding author.
E-mail address: agustin.cerezo@urv.cat (A. Cerezo).

https://doi.org/10.1016/j.radphyschem.2024.112172
Received 17 April 2024; Received in revised form 29 August 2024; Accepted 2 September 2024
Available online 5 September 2024

necessity of physically traveling to each one of the gamma spectrometry monitors with calibration sources. Moreover, these methodologies are useful for the surveillance networks of Argentina, Mexico, Paraguay and Uruguay, where we are contributing with the same very precise equipment designed and build by the Medical Physics Unit and supporting with real-time gamma-spectra analysis and data evaluation. Keep in mind the objective of these kind of environmental surveillance networks is to be able to detect presence of artificial isotopes in the environment (which we assume to be homogeneously distributed), without falling in false positive detections, and achieving MDACs as low as possible. Determine the precise activity concentration of certain isotopes is not the scope of this networks. In those cases, the network serves as a surveillance system, triggering alarms in case of nuclear accidents or releases into the environment. In those cases, other dedicated programs are activated for measuring the precise quantity of those, and other, anomalous radioisotopes (Sáez-Muñoz et al., 2024).

In this article we present the application of a new methodology adopted by the Medical Physics Unit to calibrate and analyse in real time the spectra recorded by the XVRAC monitors and other distant networks. Note that the procedure is not related to the ISO standardizations, e.g. ISO20956:2023, as the term calibration used in this article refers to a procedure that makes use of virtual spectra (instead of certified sources) to determine the correspondence between cps and activity concentration.

Additionally, we will study some detection events of artificial isotopes which activated the investigation warning level, detected by monitors where this new procedure was implemented: Detection of ^{60}Co in the vicinities of Ascó Nuclear Power Plant (N41°12′00″ E0°34′10″), detection of ^{75}Se and ^{192}Ir in the vicinity of the Vandellòs Nuclear Power Plant (N40°57′01.8″ E0°51′57.6″) (Unidad de Protección Civil, 2009) and the detection of ^{131}I in the town of Balaguer (41°47′28.21″N 0°48′39.38″E). Note that all the mentioned detections correspond to low activity concentrations, slightly above the monitors detection limits and did not pose a radiological risk for the population or the environment: detection of equal or higher values of ambient dose equivalent, H*(10), of natural isotopes (radon progeny) have been recorded during rain episodes.

2. Materials

For this study, a NaI(Tl), four $LaBr_3$(Ce) and one SrI_2(Eu) detectors, with different sizes (1″×1″ and 2″×2″), have been used, applying on them the new general calibration methodology, summarized in Fig. 5. Each one of them are in different locations. Presented below a description of them and an overview of the locations (Fig. 2).

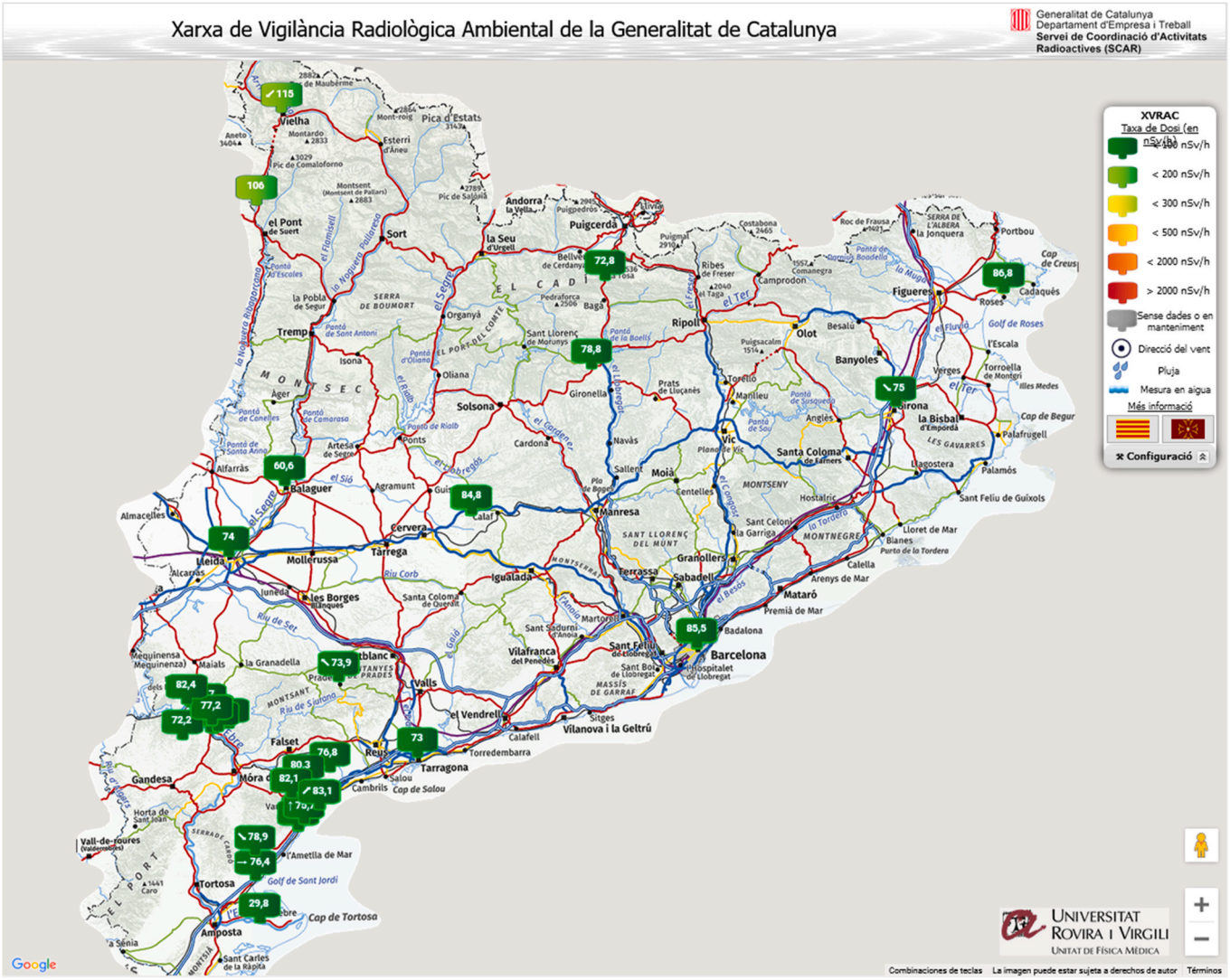

Fig. 1. General overview of XVRAC. All the monitors are showed with a green indication. The values presented show the dose rate (nSv/h) (http://xvrac.fmurv.cat/).

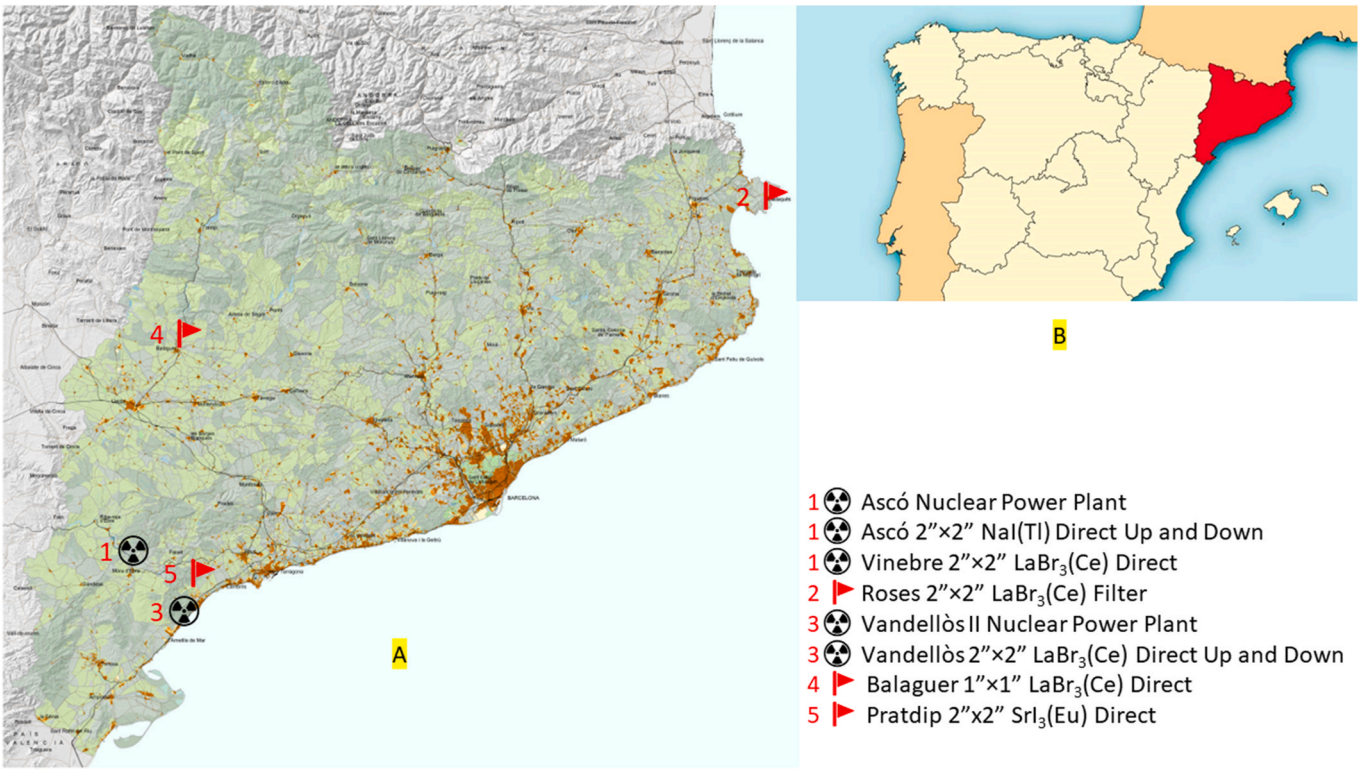

Fig. 2. A) Location of the stations for this study. Some of the monitor locations are closer than the map resolution, and so, are grouped in one point, as indicated for Ascó Nuclear Power Plant, Ascó 2″x2″ and, Vinebre 2″x2”. The Vandellòs 2″x2″ $LaBr_3$(Ce) monitor is located in the vicinity of Vandellòs nuclear power plant). B) Map of Spain showing the localization of Catalonia.

2.1. NaI(Tl) monitor

We used a monitor with two shielded 2″×2” NaI(Tl) detectors (Model 905-3 from ORTEC®), one pointing upwards and the other pointing downwards, in direct measurement configuration (Casanovas et al., 2014b), each one of them coupled to a digital multichannel analyser (Digibase from Ortec®). This monitor is located in the Ascó nuclear power plant precinct. Only the upper detector will be considered for this study, in order to compare volumetric activity concentrations with the other monitors.

2.2. $LaBr_3$(Ce) monitors

We used three monitors with four 2″×2″ $LaBr_3$(Ce) detectors (BrilLance™380 from Saint-Gobain Crystals®) coupled to digital multichannel analysers (Digibase from Ortec®). The first monitor uses one detector, and it is configured for direct measuring. This monitor is in Vinebre (N41°11′6.308″ E0°35′19.279″), a village near Ascó. Another detector is used in a particulate filter (Casanovas et al., 2014a) monitoring Roses (N42°15′47.494″ E3°10′38.638″). The last two detectors are mounted in a monitor configured for direct measurement of the upper half-plane and the lower half-plane, separately (Casanovas et al., 2014b). In this type of monitor, as in the NaI(Tl) one, a detector points upwards and the other downwards. The monitor is in Vandellòs nuclear power plant precinct. Only the upper detector will be considered for this article, in order to compare volumetric activity concentrations with the other monitors.

In addition, a 1″×1″ $LaBr_3$(Ce) (BrilLance™380 from Saint-Gobain Crystals®) coupled to a digital multichannel analyser (Digibase from Ortec®) in direct measurement configuration is installed in in Balaguer (N41° 47′ 46,2″ E0° 48’ 36.9”).

2.3. SrI_2(Eu) monitor

We used a 2″×2″ SrI_2(Eu) detector (ScintiClear™ from CapeSym®) coupled to a digital multichannel analyser (eMorpho from Bridgeport Instruments®) configured for direct measuring. This monitor is located 20 km away from Vandellòs nuclear power plant, in the village of Pratdip (N41° 3′ 3.669″ E0° 52′13.997″).

3. Methods

3.1. Spectra stabilization

Before processing the raw data, we stabilize spectra automatically using a self-developed software that applies a previously described methodology (Casanovas et al., 2012a) to avoid peak shifting in gamma spectra (Mitra et al., 2016).

3.2. Energy and FWHM(E) calibrations

Performing an energy and resolution calibration (FWHM (E)) requires the obtaining of spectra with well-defined photopeaks. To accomplish this, traditionally, spectra of radioactive calibration sources are registered in each monitoring site. This implies that technical staff must visit each monitor periodically and obtain measurements of the different radioactive sources for several minutes, as explained in (Prieto et al., 2018b). It is a time and energy consuming task, especially considering that many monitors are located in the Pyrenees mountains and require a 4-h drive to reach. To optimize this situation, we use the spectra recorded regularly by the monitors on site to calibrate the detectors (after being stabilized in temperature, as previously mentioned). To do so, we use spectra with the highest activity concentration of natural occurring isotopes in all the working period of each monitor (see Fig. 3). These spectra are valid to use as long as the detector acquisition

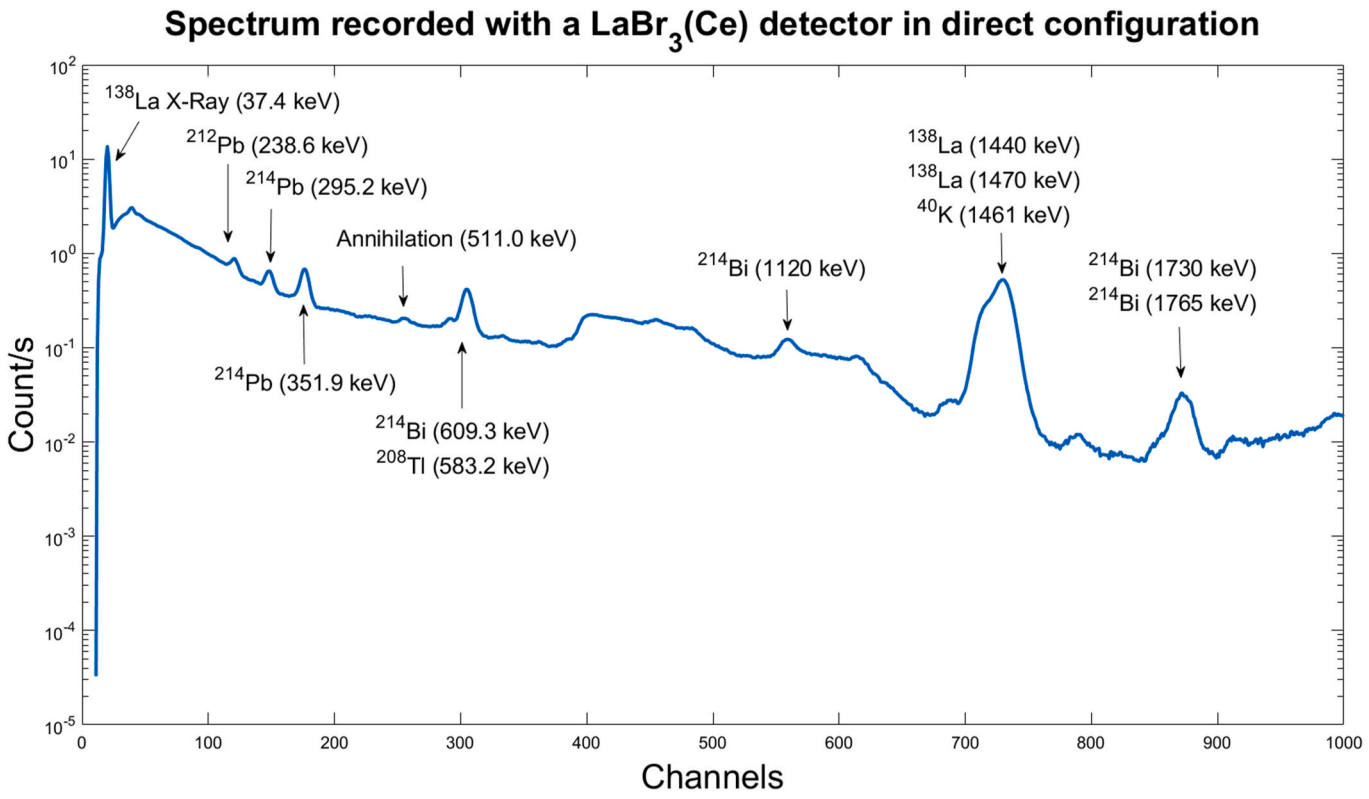

Fig. 3. Nine hours spectrum recorded by a 2″x2″ $LaBr_3$(Ce) detector in direct configuration located in Vinebre (see Fig. 2) used to calibrate in energy and resolution (FWHM(E)) the monitoring station. In the figure are presented the channels and the theoretical energy for each one of the centroid energy peaks. In this spectrum, the ^{212}Pb, ^{214}Pb and ^{214}Bi average activity concentrations were 35.1 ± 2.7, 108.7 ± 21.4 and 125.3 ± 20.9 Bq/m^3.

parameters and the monitor location remain unchanged. If an acquisition parameter or the location changes, the energy scale and the energy resolution need to be recalibrated with new spectra.

3.3. Cleaning equations

Once all the spectra have been stabilized and calibrated in energy and resolution, cleaning equations are generated to eliminate the contributions of the natural occurring radioisotopes in the spectral band of the artificial isotopes under monitoring. We developed a simple yet effective method, the proportional ROI-cleaning method, based on the analysis of regions of interest, or ROIs, as explained in (Cerezo et al., 2023). In this case, the training data correspond to the historical radioactive environmental data recorded by the desired monitors to calibrate. The cleaning equation obtained for a certain radioisotope in a certain monitor is only applicable for that isotope in that monitor while the detector acquisition parameters and the monitor location do not change. As a result, we obtain cleaned ROIs, or ROI_{Net}, where the natural isotopes contributions have been subtracted for ^{131}I, ^{137}Cs and ^{60}Co.

3.4. Efficiency calibrations

All the spectra are calibrated in efficiency to obtain activity concentrations in Bq/m^3. The efficiency calibrations are performed using Montecarlo simulations with EGS5 code, assuming the isotopes are homogeneously distributed in air.

For the aerosol monitors, it is also assumed that the distribution on the particulate filter is homogeneous (Casanovas et al., 2012b) and for the direct measurement monitors the gamma emitters are assumed to be distributed forming a cylindrical source of equal height and diameter of 500 m ('infinite' source) surrounding the detector (IAEA, 2018).

The objective with these simulations is to generate conversion factors for a hypothetic radioactive source homogeneously distributed in air in case of a nuclear accident. More details about the efficiency calculation and efficiency curves can be found in previous studies (Casanovas et al., 2012b, 2014a, 2014b; Cerezo et al., 2023), where point sources of known activity were used to validate efficiencies obtained from Montecarlo simulations.

3.5. Activity concentration

The activity concentration for isotopes of interest is calculated using the Proportional ROI-Cleaning algorithm (Cerezo et al., 2023) instead of the traditional peak analysis. Translating into activity concentration (Bq/m^3) is crucial, enabling possible comparisons with the legal limits or studies performed by other institutions (IAEA, 2018; Iaea, n.d.).

For the conversion of the counts per second (cps) in a ROI to the activity concentration (Bq/m^3), we developed the so-called *virtual spectra* method. This eliminates the need to physically transport radioactive sources to each monitoring station, as previously explained. With these spectra we begin the activity calibration procedure.

3.5.1. Virtual spectrum

Virtual spectra help avoid doing calibration procedures on site, similarly as explained in section 3.2. A virtual spectrum refers to either an artificial isotope spectrum or a natural isotope spectrum that is recorded by a detector in a laboratory, which is then validated and added to a real spectrum recorded by a remote monitor. This process enables the calibration of activity concentration.

The virtual spectrum is appliable to a certain monitor if it is recorded with the same type of detector in the laboratory (i.e.: the spectrum recorded with a 1″x1″ $LaBr_3$(Ce) detector in the laboratory cannot be applied in a 2″x2″ NaI(Tl) detector as a virtual spectrum, only is applicable to another 1″x1″ $LaBr_3$(Ce) detector). The laboratory spectrum is shifted to accommodate the emission peak in the correct channel to match the detector on field. For that, the algorithm minimizes the

difference between the experimental artificial isotope energy peak recorded in the laboratory and its theoretical energy in the field detector (see Figs. 4 and 16). This procedure is referred to as *validation*. Then this spectrum is added to a spectrum of the field detector.

3.5.2. Activity concentration calibration

Finally, we obtain the activity concentration, in Bq/m^3, for the ^{131}I, ^{137}Cs and ^{60}Co. We assume that the activity concentration, A, in Bq/m^3, is proportional to the net ROI:

$$A = a \cdot ROI_{net} \tag{1}$$

To obtain the calibration coefficient, a, we use the corresponding artificial isotope virtual spectrum to produce counts within the desired ROI. Fitting the peak of the artificial isotope to a Gaussian function allows us to obtain the height of the Gaussian, H, and the standard deviation, s, and we obtain the counts under a peak from the value of $H \cdot \sigma \cdot \sqrt{2\pi}$, which is the integral of the Gaussian function over its entire range. Then, the activity concentration is calculated for each photopeak as:

$$A = \frac{H \cdot \sigma \cdot \sqrt{2\pi}}{\varepsilon \cdot t \cdot I(\%)} \tag{2}$$

where ε is the volumetric efficiency obtained using Montecarlo simulations with isotopes homogeneously distributed in air, explained in section 3.4, t is the counting time and I (%) is the emission probability of the considered gamma-ray.

At this point, a caveat: if the virtual spectrum is added to a spectrum recorded by a field detector coinciding with a measurement with high activity concentration of natural isotopes, the gaussian fitting can overestimate the height of the energy peak due to peak overlapping and Compton scattering (e.g. ^{214}Pb and ^{131}I −351 keV and 364 keV- or ^{214}Bi and ^{137}Cs −609 keV and 661 keV-). To avoid this problem, the virtual spectrum is added to the spectrum with the lowest emission from natural occurring radioisotopes in the recorded period.

3.6. Minimum detectable activity concentration

Every 10 min a gamma spectrum is received for analysis. The uncertainty for each clean ROI can be propagated from the Poisson uncertainties of the corresponding raw ROI and the ones from the natural emitters. From these uncertainties, the detection limits for 10-min measurements are calculated following the ISO 11929 recommendations. A deeper explanation of this calculation is presented in (Cerezo et al., 2023).

To compute the MDAC after 24 h of measurements we adopt two different strategies depending on whether the detector has a particulate filter or not. In detectors with a filter (like that at Roses), we report the MDAC recorded at 23:59 every night. The reason for this is that the filter is reset every midnight. With a forced air flow of 10 m^3/h, the measurement at 23:59 has potentially sampled 240 m^3 of air and is therefore, the most significant measurement.

In direct measurement, we could in principle let the detectors accumulate a spectrum for 24h. However, we find preferrable to keep them recording short duration (10 min) spectra for the sake of temporal resolution and early-warning performance. What we can do in this case is to average the clean ROIs of the last 24 h. Every 10 min we compute the (running) average of the latest 144 10-min measurements. We can compute the uncertainty of this measurement from the propagation of the uncertainties of the 144 individual measurements and obtain the corresponding MDAC (Table 2).

3.7. Remote calibration workflow

In order to summarize the information provided in the previous sections, we present a flow chart (Fig. 5) for the steps to follow with the objective to perform an on-remote calibration for whatever gamma spectrometry monitor. Notice some steps are iterative, e.g. the spectrum stabilization, or the cleaning equation application, once the cleaning parameters are obtained, are performed for each new performed measurement, i.e. every 10 min. Other steps require being performed only once, like the Montecarlo simulations. The energy and resolution calibration curves, as well as the cleaning equations and the conversion

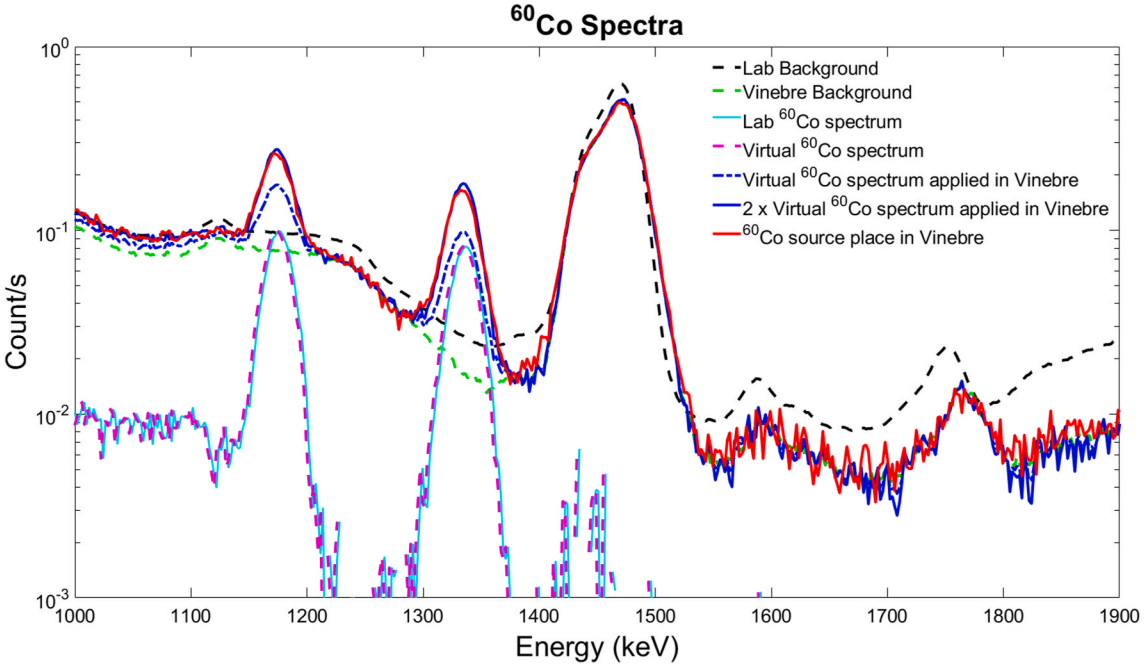

Fig. 4. Example of a ^{60}Co spectrum recorded in the laboratory (cyan line) displaced one channel to the left to obtain the ^{60}Co virtual spectrum validated for Vinebre's monitor (dashed magenta line) and applied on Vinebre's monitor (blue dotted line). To obtain the same spectrum as placing a real ^{60}Co source next to the Vinebre's monitor (red line), it is necessary to multiply by two the virtual spectrum (blue line). This is a zoom of a complete set of spectra plotted in Fig. 16.

factors, need to be recalculated every six months due to seasonal change, as explained in the **Discussion**.

4. Results

The results of applying the new calibration procedure, summarized in Fig. 5, are presented for 6 different monitors (see **Materials** section): 3 for normal natural radioactivity background monitoring (Vinebre, Roses and Pratdip; sections 4.1 and 4.2) and 3 for artificial isotopes detections (Ascó, Vandellòs and Balaguer; section 4.3).

From Figs. 6–11 we present a comparison of two different methods to analyse data registered during regular days for low and high natural isotopes activity concentration. That is, there is no presence of artificial isotopes and any radiological increase corresponds to natural isotopes. The result of subtracting an average background spectra (*Simple Background Subtraction method*) is plotted from Figs. 6–8, while from Figs. 9–11 we present the result of applying our algorithm, the Proportional ROI-Cleaning Method (Cerezo et al., 2023). The Simple Background Subtraction method returns values above zero for the three artificial isotopes studied (see from Figs. 6–8 and Table 1 which means that this method produced misleading false-positive detections. On the other hand, the Proportional ROI-Cleaning Method returns zero activity concentration for the artificial isotopes, as expected.

Figs. 12–14 show artificial isotopes detections by three different monitors where the Proportional ROI-Cleaning Method was applied. Bear in mind that there was no radiological risk to the population or to the environment.

4.1. Analysis with Simple Background Subtraction

Figs. 6–8 show the activity concentration variability of ^{212}Pb, ^{214}Pb and ^{214}Bi and its effect on the ROIs of the artificial isotopes if the data are analysed with a Simple Background Subtraction method (i.e. this method relates the counts in each studied artificial isotope's emission peak to the activity concentration after applying a Gaussian fitting which only subtracts the intrinsic background and the constant background, but not the contributions from natural isotopes to the artificial isotopes emission peaks due to Compton scattering or peaks overlapping) for three different stations. The method has been applied on periods with low and high natural isotopes activity concentration, specially selected for each monitor.

4.2. Analysis with proportional ROI-cleaning method

Figs. 9–11 show the resulting activity concentration of the three artificial isotopes studied (^{131}I, ^{137}Cs and ^{60}Co) once our method (Cerezo et al., 2023), that subtracts the contributions of the natural isotopes to the ROIs under monitoring, is applied to the same data presented in section 4.1.

In Table 1 the results obtained with our method (proportional ROI-cleaning method) and the Simple Background Subtraction method, are summarized for each detector. In Table 2, the mean Minimum Detectable Activity Concentrations (MDAC) of the artificial isotopes are presented for the three detectors.

4.3. Detections of interest

In general, our monitoring stations routinely record artificial isotopes activity concentration values of zero (Table 1). However, in some special cases we have detected actual measurements of artificial isotopes with no radiological impact to the population or the environment with values slightly above the monitors' detection limits. Some of such rare

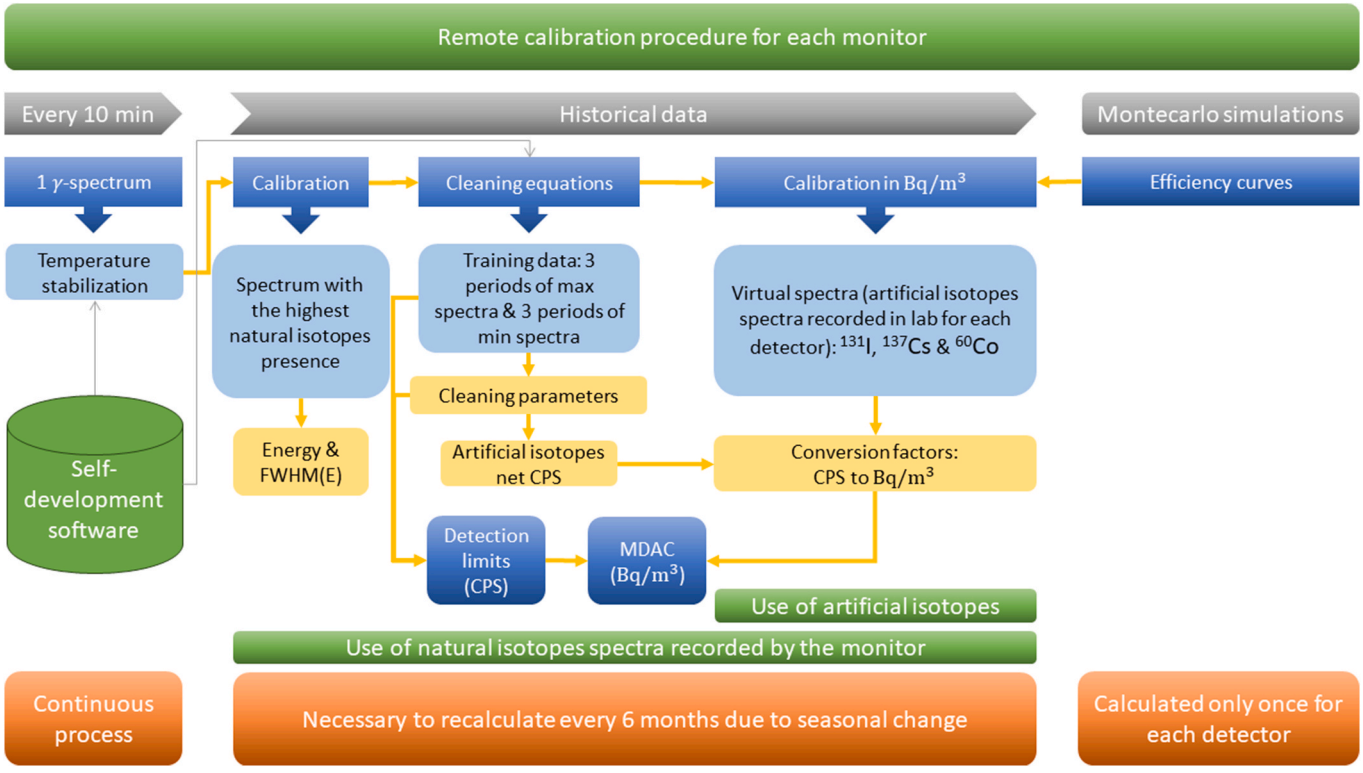

Fig. 5. Flow chart of the complete remote calibration procedure performed for each one of the monitors, which is divided in three main steps: 1) Every 10 min, each spectrum is stabilized in temperature (Casanovas et al., 2012a). 2) The historical data recorded by a monitor (natural isotopes spectra) is used to: Self-calibrate it in energy and resolution, to generate the cleaning equations, i.e. the corresponding cleaning parameters (Cerezo et al., 2023), obtaining the artificial isotopes net counts, and to obtain the detection limits in counts per second (CPS). 3) Montecarlo simulations are performed to obtain the corresponding efficiency curves (Casanovas et al., 2012b, 2014a, 2014b; Cerezo et al., 2023). 4) The monitor is calibrated in Bq/m^3 remotely applying virtual spectra (the concept of virtual spectra was explained in section 3.5.1), obtaining the conversion factors, as explained in section 3.5.2.

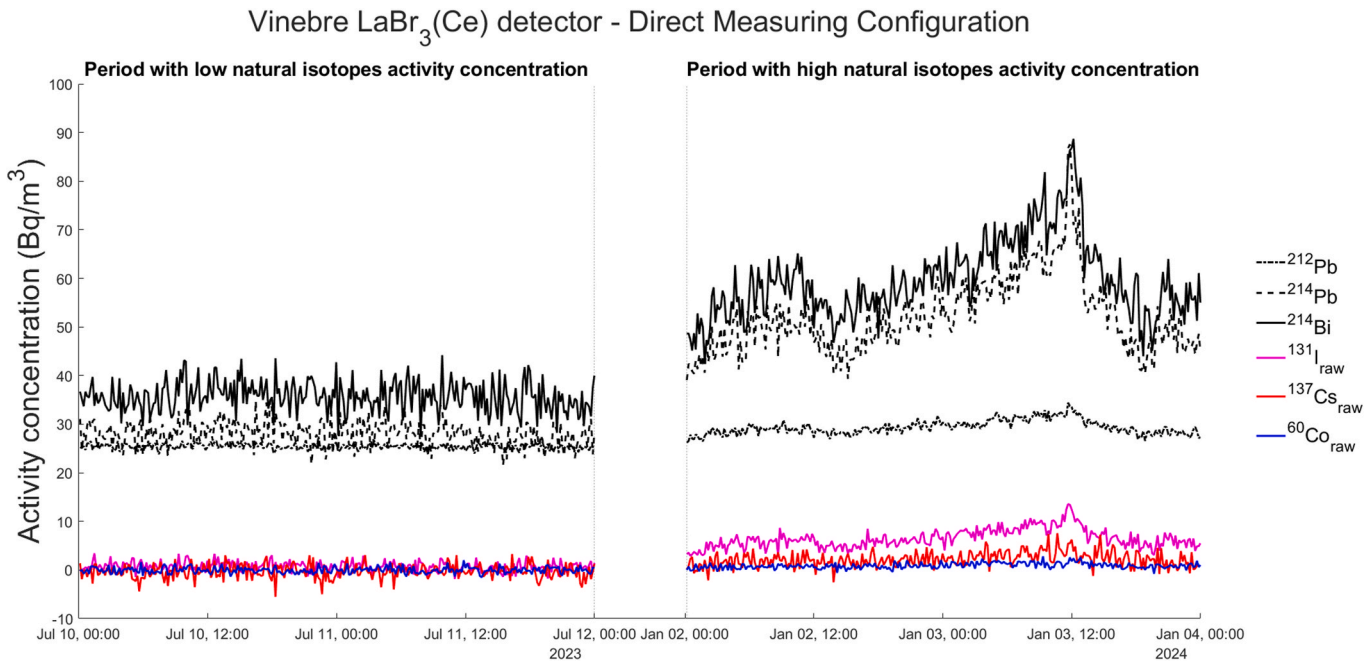

Fig. 6. Raw data for the Vinebre $LaBr_3(Ce)$ detector in direct measuring configuration on a scenario of variable natural radioactivity affecting the detection of artificial radioisotopes if the Simple Background Subtraction method is applied. The high natural period corresponds to raining events.

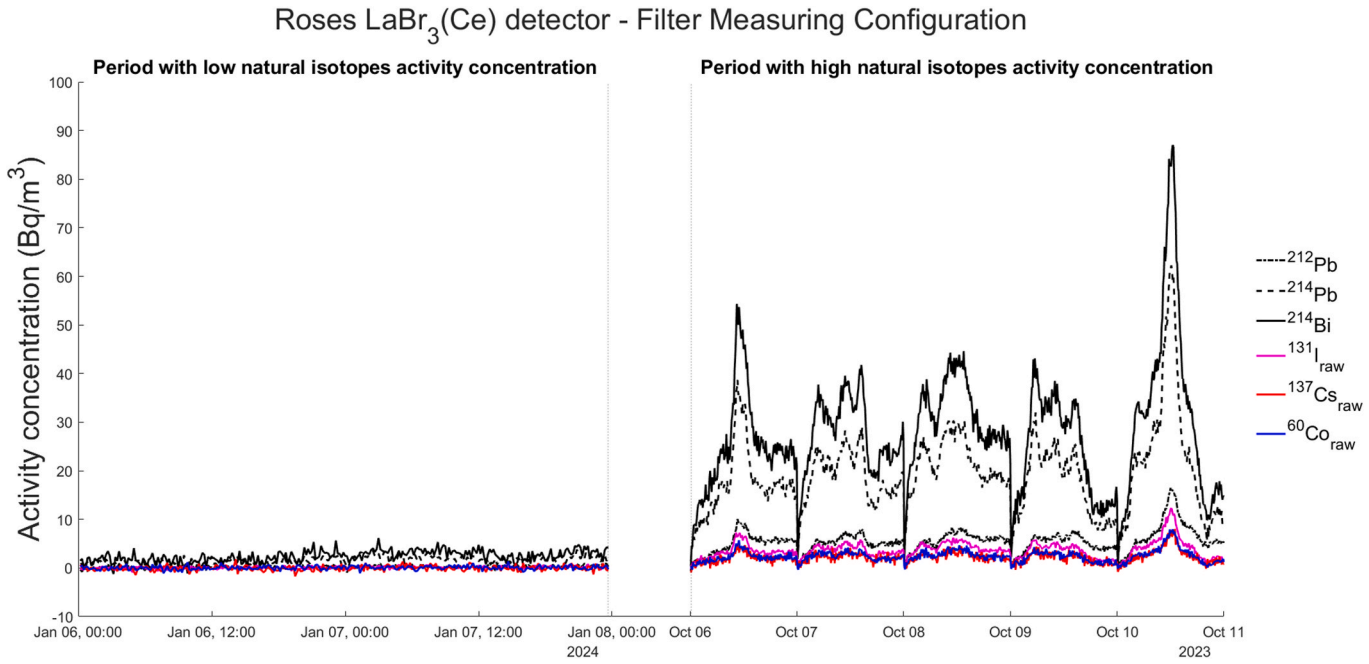

Fig. 7. Raw data for the Roses $LaBr_3(Ce)$ detector in filter measuring configuration on a scenario of variable natural radioactivity affecting the detection of artificial radioisotopes if the Simple Background Subtraction method is applied. The high natural period corresponds to radon emanations events.

events are discussed below (See Appendix I for the waterfall spectra representation of the detections) where the remote calibration procedure (see Fig. 5) has been applied.

4.3.1. *Ascó - Shielded 2″x2″ NaI(Tl) detector*

This monitor is located in the site of the Ascó Nuclear Power Plant. We present two detections of ^{60}Co recorded in short events in 2023. After contacting the pertinent authorities, it was determined that the presence of ^{60}Co corresponded to an authorized truck carrying shielded paraffin canisters with ^{60}Co inside them. The truck passed within 70 m of the detectors. This transportation did not pose a risk to the population or the environment. The detection recorded in January, generated an increase in the H*(10) of 10 nSv/h - from a background level of 80 nSv/h, while the detection in February generated an increment of 12 nSv/h. Bear in mind that these occasional increases are similar to those generated in a rainfall event.

4.3.2. *Vandellòs - Shielded 2″x2″ $LaBr_3(Ce)$ detectors*

This monitor is located in the vicinity of Vandellòs Nuclear Power Plant. On July 27th, 2020, it was detected presence of ^{75}Se (mainly

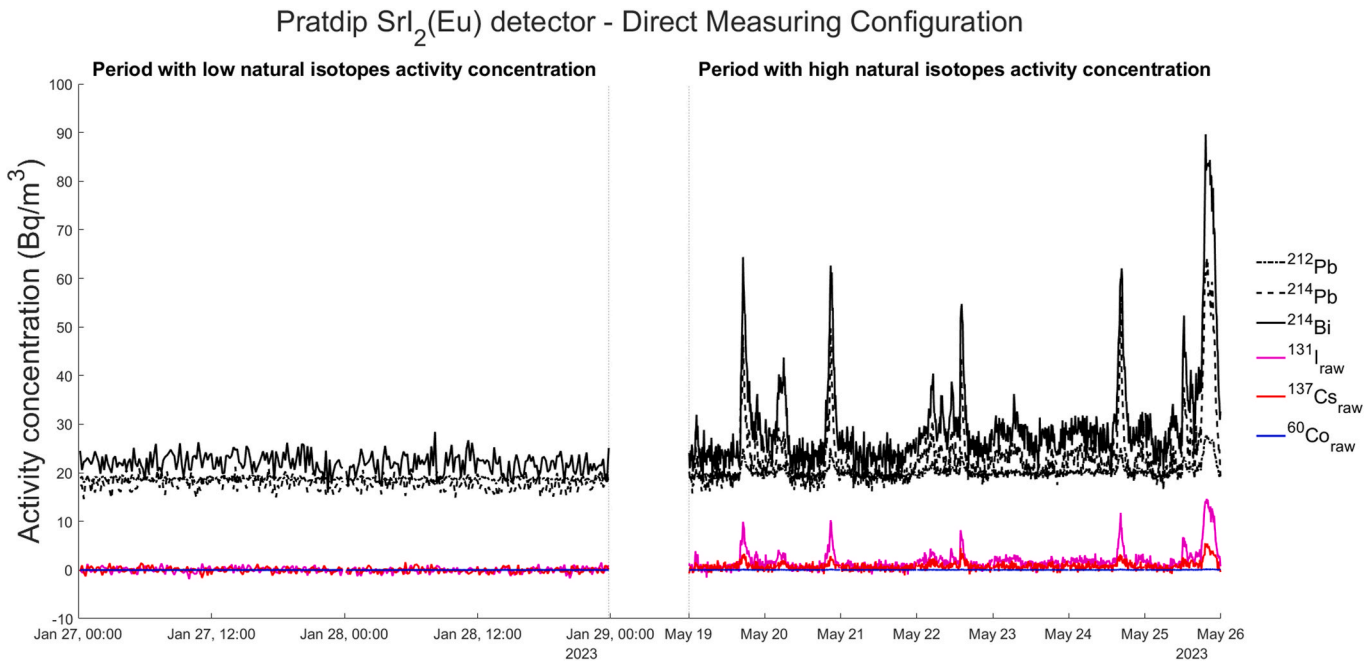

Fig. 8. Raw data for the Pratdip $SrI_2(Eu)$ detector in direct measuring configuration on a scenario of variable natural radioactivity affecting the detection of artificial radioisotopes if the Simple Background Subtraction method is applied. The high natural period corresponds to raining events.

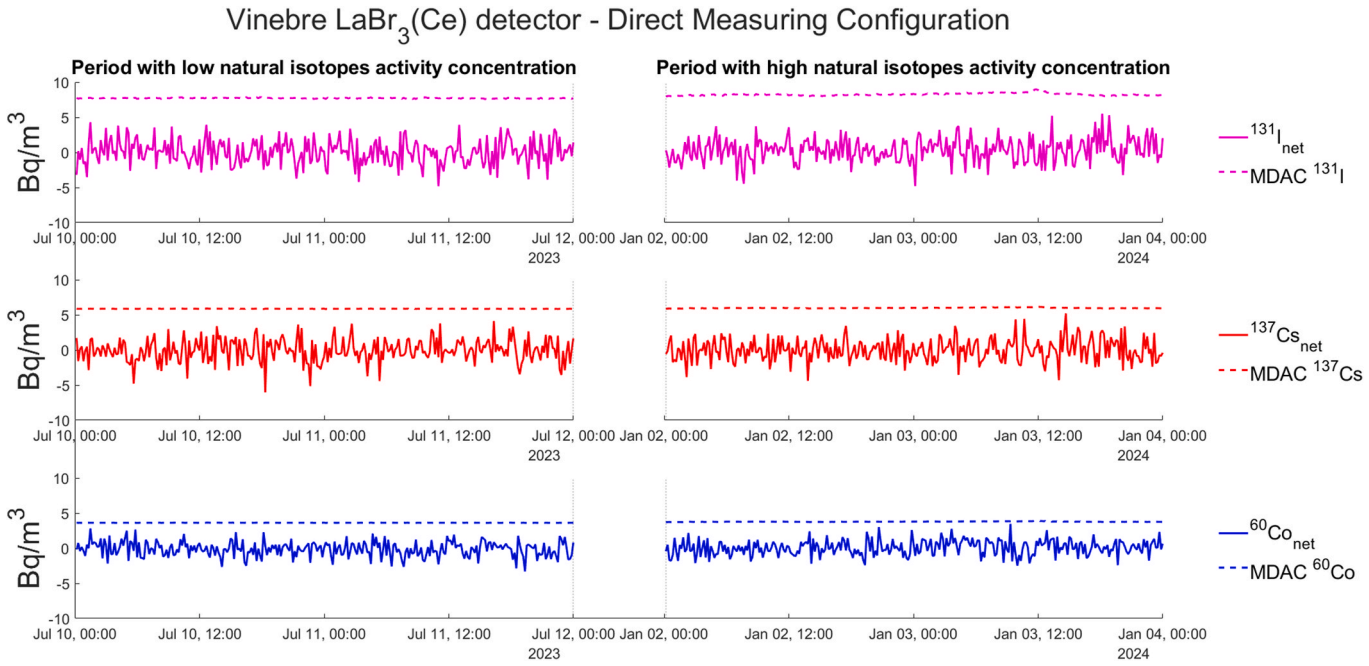

Fig. 9. Net data and MDAC for the Vinebre $LaBr_3(Ce)$ detector in direct measuring configuration (same detector as used in Fig. 6) in the same scenarios after applying our developed algorithm. The high natural period corresponds to raining events.

γ-emissions: 121.12, 136.00, 264.66, 279.54 and 400.66 keV) and ^{192}Ir (mainly γ-emissions: 295.96, 308.46, 316.51 and 468.07 keV). Once contacting the pertinent authorities, it was determined that the presence of this artificial radioisotopes corresponded with an authorized industrial scintigraphy. In this station, there are no ROIs defined for those isotopes. However, these radioisotopes generate Compton scattering, affecting the ^{131}I (main γ-emission at 364.5 keV) ROI, producing a positive signal in the ^{131}I ROI (see the waterfall in Fig. 15b of Appendix I). The detection generated an increase of 10 nSv/h from the background level (110 nSv/h).

4.3.3. *Balaguer - 1″×1″ $LaBr_3(Ce)$ detector*

A 1″×1″ $LaBr_3(Ce)$ direct measurement configuration monitor is located in the rooftop of a sports centre in the city of Balaguer. On January 26th, 2023, ^{131}I was detected. On that day, there was a festive lunch gathering more than 200 attendees at the sports centre. Upon contacting the sports centre staff for additional information regarding the event, they informed us that some participant may have undergone a medical procedure requiring the use of ^{131}I. The detection generated an increase of 21 nSv/h from the background level (66 nSv/h).

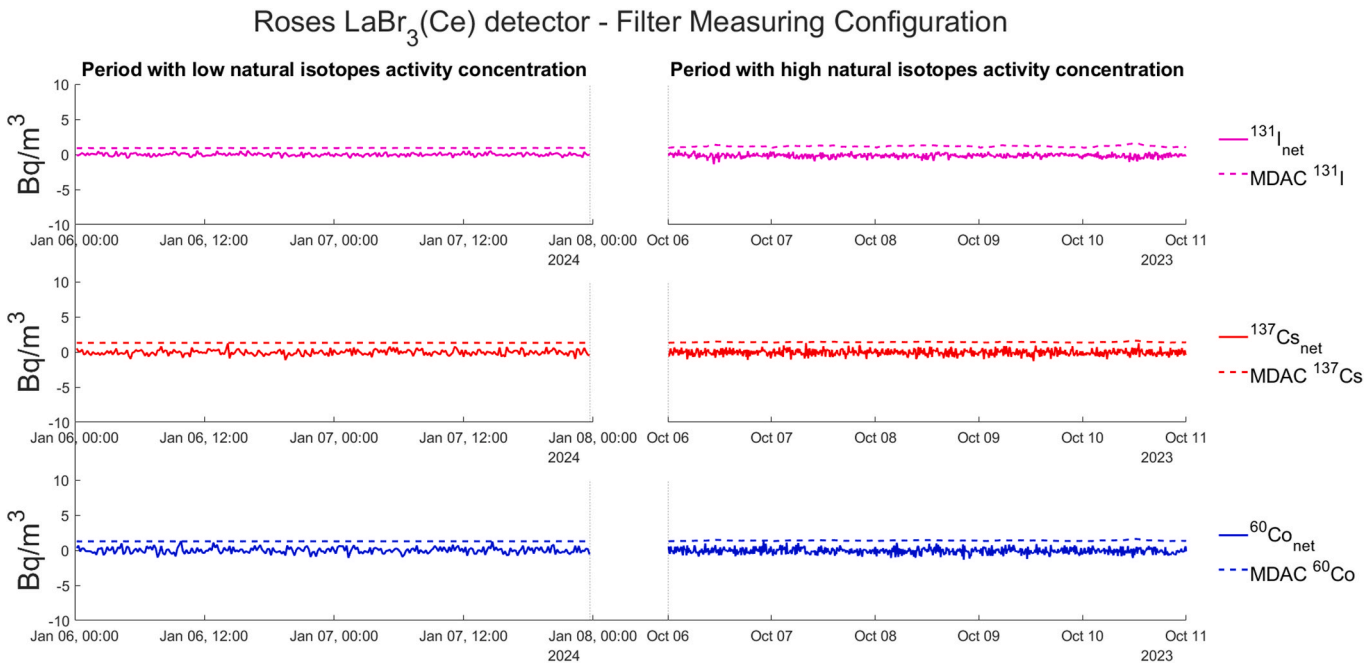

Fig. 10. Net data and MDAC for the Roses $LaBr_3(Ce)$ detector in filter measuring configuration (same detector as used in Fig. 7) in the same scenarios after applying our developed algorithm. The high natural period corresponds to radon emanations events.

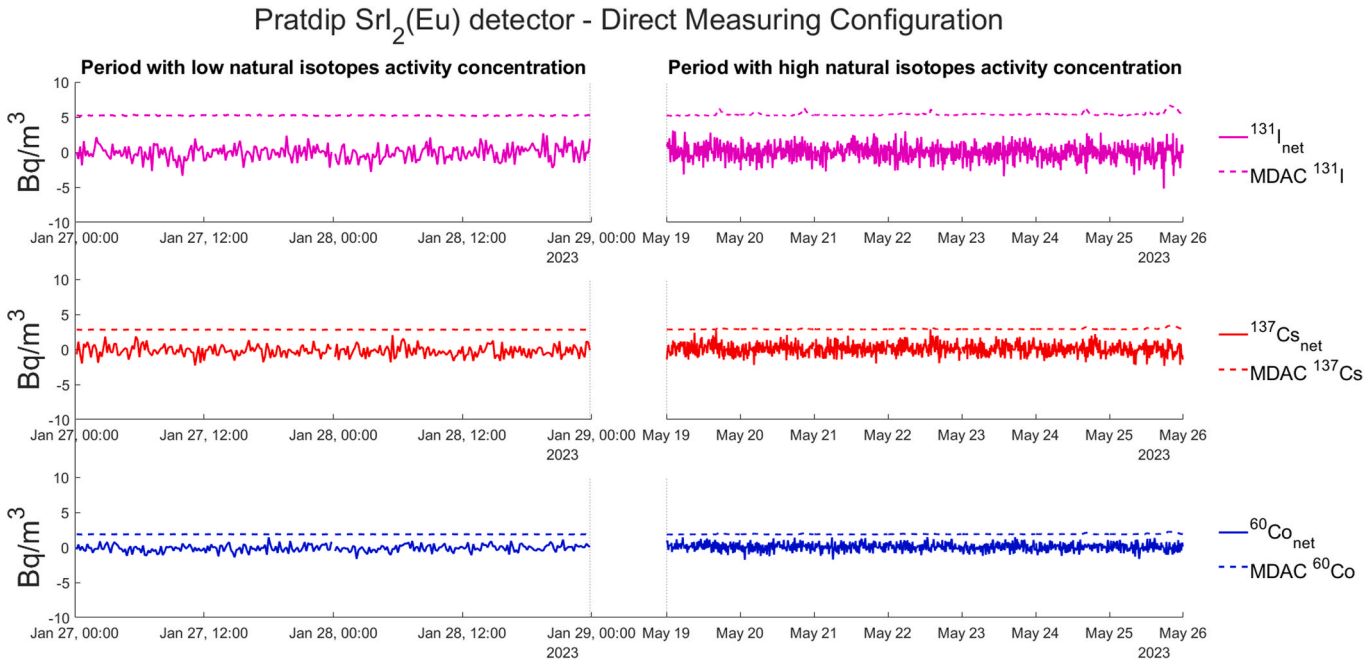

Fig. 11. Net data and MDAC for the Pratdip $SrI_2(Eu)$ detector in direct measuring configuration (same detector as used in Fig. 8) in the same scenarios after applying our developed algorithm. The high natural period corresponds to raining events.

5. Discussion

This article presents a new procedure capable of remotely calibrating gamma spectrometry monitors. While the procedure has been developed for a general application, certain considerations must be noted, and others discussed.

5.1. Energy and resolution calibration

As explained in section 3.2, this step, is traditionally performed with spectra of radioactive calibration sources obtained using point-like sources on the monitoring site. As mentioned, our group decided to optimize this practice, using the spectra recorded regularly by the monitors on site to calibrate the detectors. For this purpose, we use spectra with the highest activity concentration of natural occurring isotopes in all the working period of each monitor.

It is imperative to remark that the spectra used to calibrate in energy and resolution are valid to use as long as the detector acquisition parameters and the monitor location remain unchanged. If an acquisition parameter or the location changes, the energy scale and the energy

Table 1
Mean activity concentration values for the respective artificial isotope obtained with the Proportional ROI-Cleaning method or the Simple Background Subtraction, recorded in 10 min acquisitions with a $LaBr_3$(Ce) monitor in direct measuring configuration (Vinebre), a $LaBr_3$(Ce) monitor in filter measuring configuration (Roses) and a SrI_2(Eu) monitor in direct measuring configuration (Pratdip) for the period of low and high natural isotopes activity concentration.

	Simple Background Subtraction (Bq/m^3)			Proportional ROI-cleaning Method (Bq/m^3)		
	^{131}I	^{137}Cs	^{60}Co	^{131}I	^{137}Cs	^{60}Co
Period with low natural isotopes activity concentration						
$LaBr_3$(Ce) Direct	0.72 ± 1.05	−0.30 ± 1.45	−0.11 ± 0.51	−0.02 ± 1.77	−0.09 ± 1.64	−0.13 ± 1.09
$LaBr_3$(Ce) Filter	0.07 ± 0.27	−0.04 ± 0.53	0.05 ± 0.41	−0.03 ± 0.35	−0.11 ± 0.60	−0.01 ± 0.67
SrI_2(Eu) Direct	0.00 ± 0.59	−0.00 ± 0.55	0.00 ± 0.02	−0.12 ± 1.04	−0.21 ± 0.77	−0.11 ± 0.49
Period with high natural isotopes activity concentration						
$LaBr_3$(Ce) Direct	6.48 ± 1.96	2.20 ± 1.60	0.90 ± 0.59	0.04 ± 1.73	0.09 ± 1.59	0.07 ± 1.10
$LaBr_3$(Ce) Filter	3.74 ± 1.76	2.22 ± 1.24	2.44 ± 1.25	−0.29 ± 0.47	−0.12 ± 0.69	−0.16 ± 0.68
SrI_2(Eu) Direct	1.19 ± 2.21	0.82 ± 0.86	0.03 ± 0.03	−0.08 ± 1.11	−0.07 ± 0.82	−0.05 ± 0.55

Table 2
Mean MDAC values obtained for ^{131}I, ^{137}Cs and ^{60}Co after the application of the Proportional ROI-Cleaning method on a $LaBr_3$(Ce) monitor direct measuring configuration (Vinebre), a $LaBr_3$(Ce) monitor in filter measuring configuration (Roses) and a SrI_2(Eu) monitor in direct measuring configuration (Pratdip) for the period of low and high natural isotopes activity concentration.

	MDAC 10 min measurement (Bq/m^3)			MDAC 24 h measurement (Bq/m^3)		
	^{131}I	^{137}Cs	^{60}Co	^{131}I	^{137}Cs	^{60}Co
Period with low natural isotopes activity concentration						
$LaBr_3$(Ce) Direct	7.73	5.78	3.63	0.63	0.47	0.30
$LaBr_3$(Ce) Filter	1.30	1.85	1.79	0.006	0.009	0.009
SrI_2(Eu) Direct	5.22	2.86	1.83	0.43	0.23	0.15
Period with high natural isotopes activity concentration						
$LaBr_3$(Ce) Direct	8.26	5.93	3.73	0.68	0.49	0.31
$LaBr_3$(Ce) Filter	1.66	2.00	1.95	0.007	0.009	0.009
SrI_2(Eu) Direct	5.48	2.93	1.91	0.45	0.24	0.16

resolution need to be recalibrated with new spectra. Furthermore, the experience gained managing the surveillance network showed that it is recommendable to perform a new energy-resolution calibration every six months, prompted by the seasonal changes.

5.2. Cleaning equations

The cleaning equations, as mentioned in section 3.3, need a set of spectra only with presence of natural isotopes. Moreover, the datasets need to be created with maximum and minimum spectra due to natural isotopes activity concentrations among all the spectra recorded by the monitor. Spectra with intermediate values (i.e. natural isotopes activity concentrations between the max and min historically recorded values) can be added in the data set, which will improve the result.

However, while this last point is recommendable, creating the data sets with the maximum values recorded is necessary. The use of maximum values generate cleaning equations to avoid false positive detections of artificial isotopes in case of an event with high natural isotopes activity concentrations. For instance, let us consider the detection in Sellafield (Office for Nuclear Regulation, n.d.), where the systems produced a false-positive detection of artificial isotopes released into the environment that was caused by Radon emanation. Furthermore, to prevent this undesired result, the maximum spectra ever recorded by a monitor is used as a virtual spectrum of natural isotopes to simulate events twice or three times more intense. These natural high intensity spectra are added to the data used to determine the cleaning equations. Thus, the procedure is capable of accurately obtaining results, even in a worst-case scenario, without producing false-positive detections.

Note that the datasets are valid as long as the acquisition parameters of the monitor and the surroundings do not change. Again, the experience obtained in the surveillance network showed that is recommendable to generate new cleaning equations every six months, due to seasonal changes. A minimum of 3 months is necessary to generate enough data to obtain proper cleaning equations.

5.3. Virtual spectrum and activity concentration calibration

A virtual spectrum is only valid to be applied on monitors that use the same kind of detector as the one in the laboratory. i.e. it is not correct to apply a virtual spectrum recorded in the laboratory with a NaI(Tl) on a monitor with a $LaBr_3$(Ce). Also, if the energy calibration of a monitor changes, the virtual spectrum must be revalidated following the steps presented in section 3.5.1. This will also affect the activity concentration calibration, therefore, new CPS to Bq/m^3 conversion factors must be obtained.

The concept of virtual spectrum is not limited to the obtention of artificial isotopes gamma spectra, but also embraces the obtention of natural isotopes gamma spectra. As mentioned, these spectra can be applied to other stations provided that the monitors have the same type of detector. To prepare a virtual spectrum, we can use spectra obtained with radioactive point-like sources either with laboratory or on-field detectors. The recorded spectra can be used as virtual spectra for other equal detector types. In the case of the natural isotopes, virtual gamma spectra are obtained for each field monitor using periods with the highest activity concentration of natural isotopes, usually coinciding with raining events. It is not possible to apply these spectra to other monitors due to the difference of natural isotopes proportions from the surroundings of one station to another.

For each monitor, the virtual spectra library is valid while the acquisition parameters, the monitor configuration and/or the location of the monitor do not change.

5.4. Results

The procedure presented in this article, summarized in Fig. 5, has been applied to the totality of the monitors that build the environmental surveillance network of Catalonia. In this article, six monitors are presented: In sections 4.1 and 4.2 three monitors are used to show the difference in the results of applying the algorithm developed by (Cerezo et al., 2023) (Figs. 9–11) or without applying the algorithm following traditional background subtraction methods (Figs. 6–8) in presence of variable natural radioactivity for low and high natural isotopes activity concentrations. In section 4.3 three other monitors show the potential of the gamma spectrometry, being able to detect the presence of artificial isotopes, where the obtained H*(10) increments returned values below the notification level (Casanovas et al., 2011), i.e., 12, 10 and 21 nSv/h vs background of 80, 110 and 114 nSv/h, respectively. Note that the monitoring network has recorded much higher values of natural origin correlated with rain events. For instance, the natural isotopes activity concentration showed in Fig. 6, corresponds with a maximum value of 76 nSv/h.

The monitors' volumetric efficiency curves have been obtained by Montecarlo simulations, assuming a homogenously distributed source in the air (Casanovas et al., 2014a, 2014b). The sources that generated the

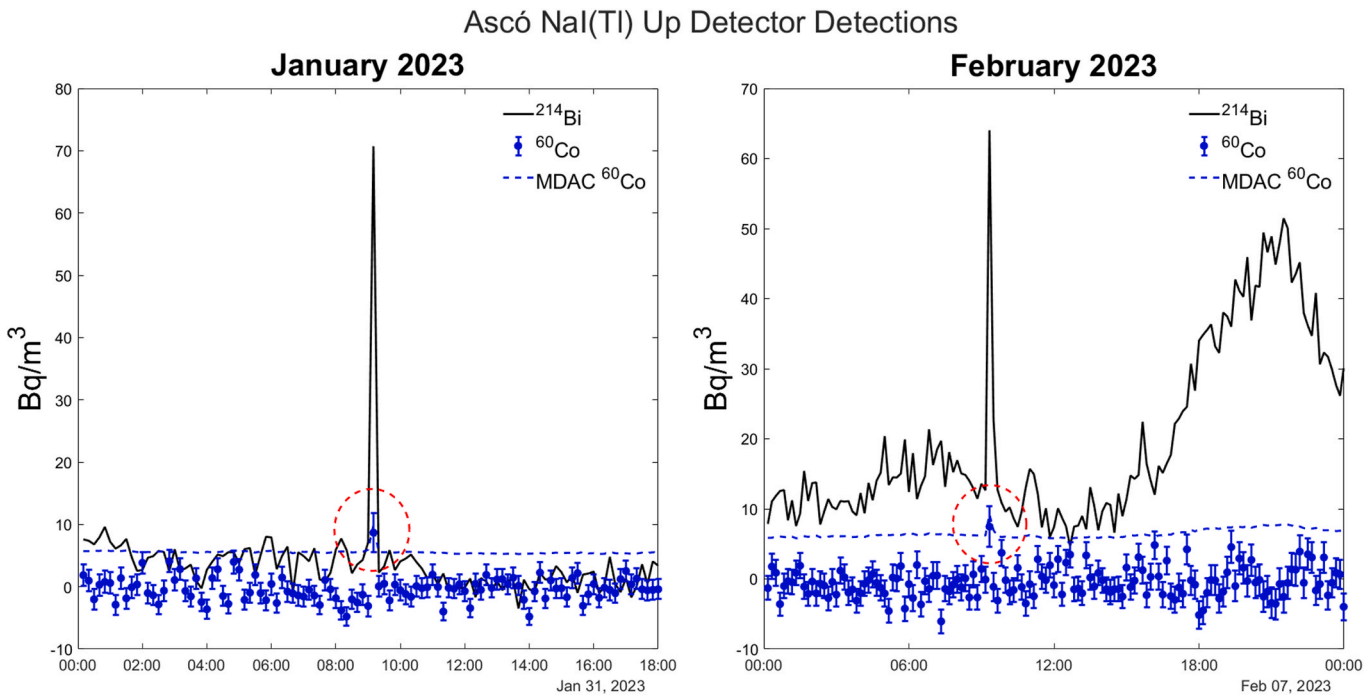

Fig. 12. ^{60}Co detections observed in Ascó station (upwards detector), indicated with a red circle. The ^{60}Co values correspond to those obtained after applying the corresponding cleaning equation. For an easier data view, only the ^{214}Bi is plotted. The apparent spike in ^{214}Bi is due to the comptonization of the gamma rays from the ^{60}Co. In the February event, can be seen a wide peak at, approximately, 21:00 h. This peak is generated only by the natural isotopes' contributions.

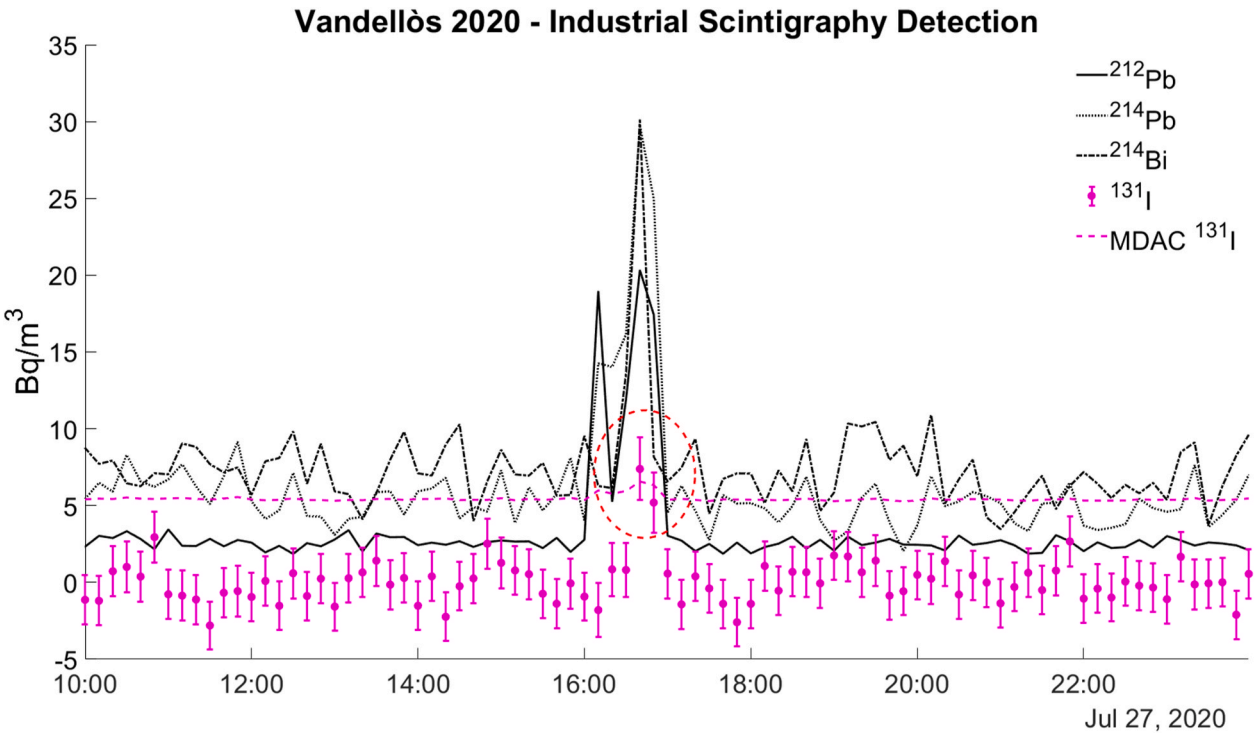

Fig. 13. ^{131}I increment observed in Vandellòs station, indicated with a red circle. The ^{131}I values correspond to those obtained after applying the corresponding cleaning equation. Only the pointing-up detector results are shown.

events showed in Figs. 12–14, can be treated as point-like sources due to the detector-source distance. Therefore, the activities showed do not correspond with a diffuse source. However, their activity was high enough to generate a signal increase above the background, being detectable by our systems with only 10 min measurement spectra. The objective of this environmental surveillance network is to be able to detect presence of artificial isotopes in the environment (which we assume to be homogeneously distributed), without falling in false positive detections, and to achieve MDACs as low as possible. The determination of the precise activity concentration of certain isotopes is not the scope of the network. The network serves as a surveillance system to trigger alarms in case of nuclear accidents or releases into the environment. If

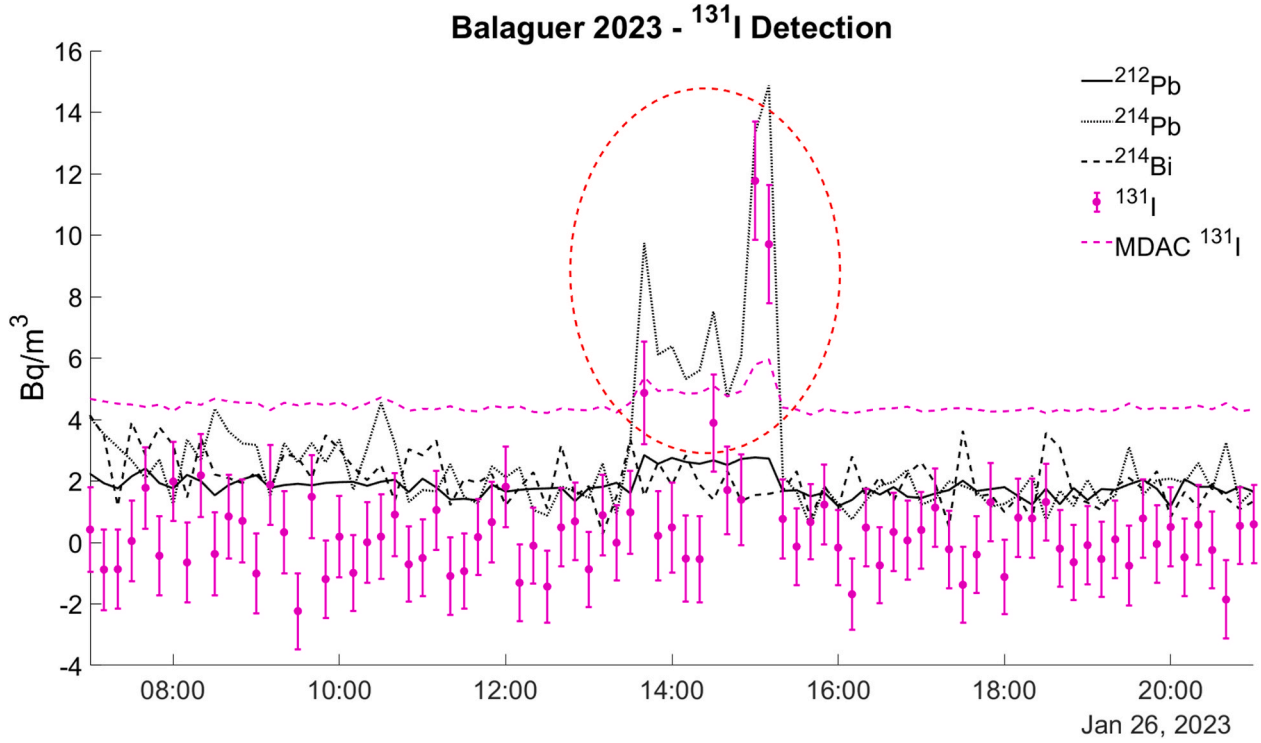

Fig. 14. ^{131}I detection observed in Balaguer sports centre, indicated with red circles. The ^{131}I values correspond to those obtained after applying the corresponding cleaning equation.

necessary (and bearing in mind that this is not the objective of this work) for a specific event, Monte Carlo simulations could be redone to allow a more accurate quantification of the activity concentration, provided that realistic information on the source term is available.

5.4.1. *Detections of interest*

The analysis of the events showed in this section regarding the natural occurring radioisotopes is very interesting. As can be observed in Figs. 12–14, the ^{212}Pb, ^{214}Pb and ^{214}Bi activity concentration suffers an apparent increment in the precise moment that the artificial isotope activity concentration rises. In Fig. 12, the increments were due to the scattering produced by the resin canisters plus the Compton effect. In Fig. 13, we have a similar situation, with the peculiarity of the peak on the left, where we cannot see an increment in the ^{131}I activity. This is caused by the most intense emission lines of ^{75}Se (264.65 keV with an I (%) = 58.9%) and ^{192}Ir (316.50 keV with an I(%) = 82.86%) which are below the ^{131}I emission peak at 364.48 keV. The increase of ^{214}Bi (609 keV) is produced due to the ^{192}Ir emission peaks at 604.41 keV (I(%) = 8.2%) and 612.46 keV (I(%) = 5.34%). Obviously, the measurement of ^{214}Pb (351 keV) was also affected. In Fig. 14, the ^{214}Pb is the most affected, due to the ^{131}I peak overlapping. In this case, the ^{214}Bi remains invariable and the ^{212}Pb suffers a low increase, attributed to the Compton effect. It must be noted that the Compton effect produced by the artificial isotopes generated an apparent increase in the natural isotopes activity concentration, which implied an increase of the MDAC. However, the three events were detectable and real-time identified.

6. Conclusions

In this article, we present a new methodology that makes possible to calibrate remotely the different gamma spectrometry detectors of the Catalan gamma spectrometry surveillance network (see flow chart on Fig. 5). We have implemented an algorithm that enables the detection and quantification of artificial isotopes in the environment, subtracting the possible variable natural radioisotopes contributions and the constant background in real-time gamma spectrometry measurements. We also obtained the corresponding MDAC for each measurement (Cerezo et al., 2023) and the 24 h MDAC.

The proposed methodology presents great advantages by eliminating the necessity to travel to each gamma spectrometry station with radioactive sources, using instead virtual spectra for the desired artificial isotope. This methodology has been applied regardless of the monitor and detector crystal types as it was implemented for four $LaBr_3$(Ce), a SrI_2(Eu) and a NaI(Tl) detectors, in different measuring configurations. Therefore, it is expected to be easy to implement in other real-time gamma spectrometry networks using scintillation detectors.

Studying the ^{131}I, ^{137}Cs and ^{60}Co (main indicators of a nuclear accident) enables to monitor other spectral bands at low, medium and high emission energies where cleaning equations are not specifically developed, as the Vandellòs event (see section 4.3.2). When in presence of other artificial isotopes, the system produces a false-positive detection in one or more spectral bands of the studied isotopes (^{131}I, ^{137}Cs and ^{60}Co) due to Compton scattering. In those cases, an in-depth study is necessary through the waterfall disposal and single gamma spectra to determine the origin of the anomalous values (see Fig. 15).

However, recently, new methodologies developed by our group, based on the stripping spectra concept, are better to obtain suitable cleaning equations for low-energy emission artificial isotopes, while obtaining similar results for medium and high energy emission artificial isotopes. This will be discussed in future works.

CRediT authorship contribution statement

A. Cerezo: Writing – review & editing, Writing – original draft, Visualization, Validation, Software, Methodology, Investigation, Formal analysis, Data curation, Conceptualization. **I. Reichardt:** Writing – review & editing, Writing – original draft, Visualization, Validation, Software, Methodology, Investigation, Formal analysis, Data curation, Conceptualization. **E. Prieto:** Writing – review & editing, Writing – original draft, Validation, Supervision. **R. Casanovas:** Writing – review

& editing, Supervision. **C. Rovira:** Writing – review & editing. **M. Salvadó:** Writing – review & editing, Writing – original draft, Visualization, Validation, Supervision, Resources, Project administration, Methodology, Investigation, Formal analysis, Data curation, Conceptualization.

Declaration of competing interest

The authors declare the following financial interests/personal relationships which may be considered as potential competing interests:A. Cerezo, I. Reichardt, E. Prieto, R. Casanovas and M. Salvado reports equipment, drugs, or supplies was provided by Servei de Coordinació d'Activitats Radioactives (SCAR, Radioactive Activities Coordination Service). C. Rovira reports a relationship with Servei de Coordinació d'Activitats Radioactives (SCAR, Radioactive Activities Coordination Service) that includes: employment. The authors declare that they have no known competing financial interests or personal relationships that could have appeared to influence the work reported in this paper. If there are other authors, they declare that they have no known competing financial interests or personal relationships that could have appeared to influence the work reported in this paper.

Data availability

Data will be made available on request.

Acknowledgments

This research was performed using data from the radiological network of Servei de Coordinació d'Activitats Radioactives (SCAR, Radioactive Activities Coordination Service) of the Generalitat de Catalunya.

Appendix IWaterfall dispositions

In Fig. 15 we present the waterfall spectra representation, where the horizontal axis is energy and the vertical axis is time (advancing upwards). This cascade representation aims to show many spectra at once, seen from above. The colour scale is the intensity of each energy channel for each spectrum. This representation highlights sudden increases in photopeaks, but also the enhanced comptonization at energies lower than the primary emitter. The waterfall is therefore useful to identify artificial isotopes that are not expressly under monitoring, but also to understand the effect of the enhanced emission in the ROIs of lower energy.

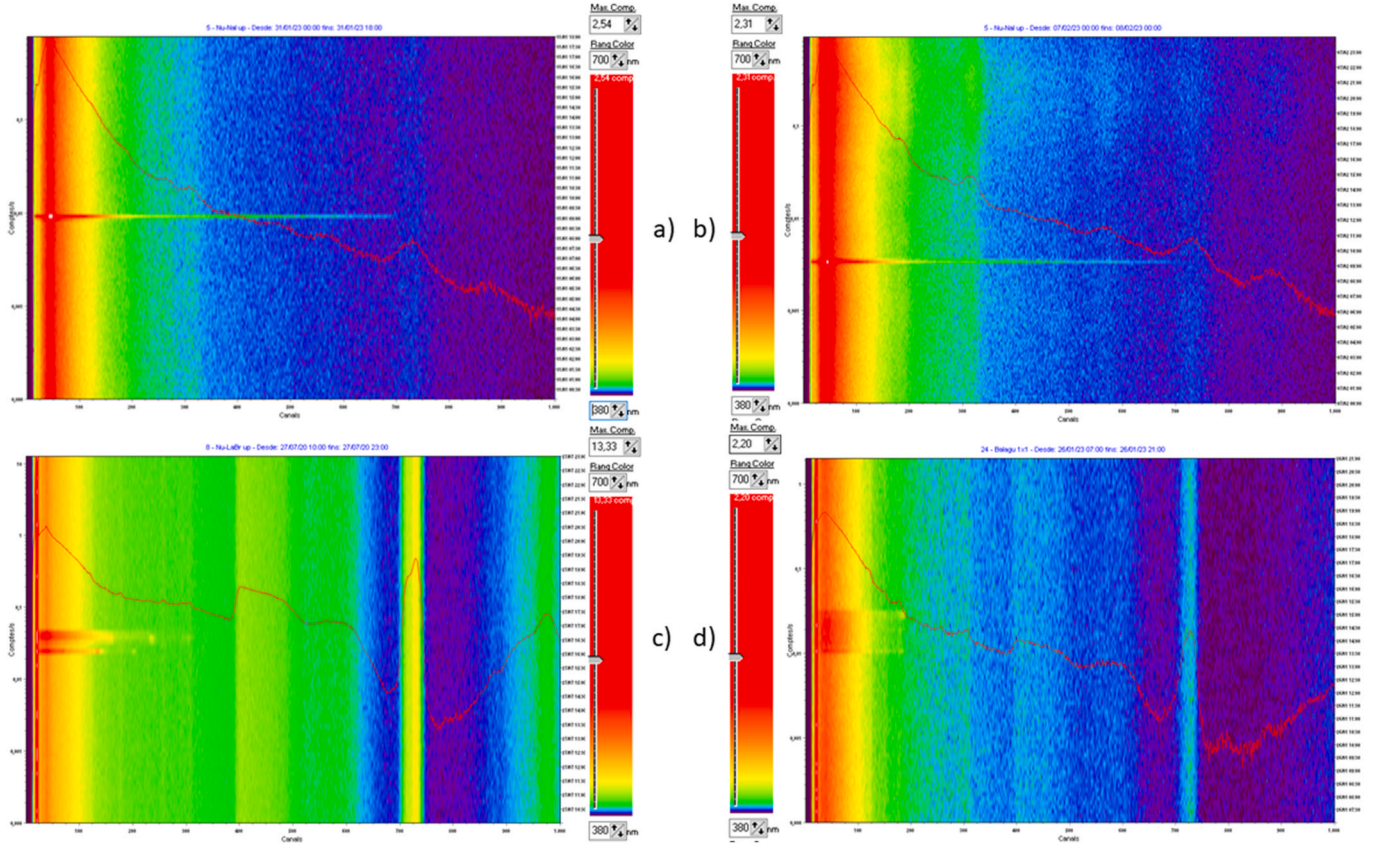

Fig. 15. Waterfall representation for the three stations showed in section 4.3. Figures a) and b) are the Ascó the spectra recorded with the NaI(Tl) detector and the corresponding detections showed in Fig. 12. Figure c) is the Vandellòs spectra recorded with the $LaBr_3$(Ce) detector showing the ^{75}Se and ^{192}Ir presented in Fig. 13. Figure d) is the Balaguer spectra recorded with the $LaBr_3$(Ce) detector showing the ^{131}I detections presented in Fig. 14.

Appendix II. Complete spectra visualization

In Fig. 16 we present a complete visualization of the spectra involved in Fig. 4. The laboratory and Vinebre's monitor backgrounds are plotted as well as the ^{60}Co spectrum recorded in the laboratory, being validated and being applied on Vinebre's monitor. As can be observed, applying and operating properly a virtual spectrum returns the same spectrum as placing a ^{60}Co source next to the Vinebre's monitor (blue and red lines).

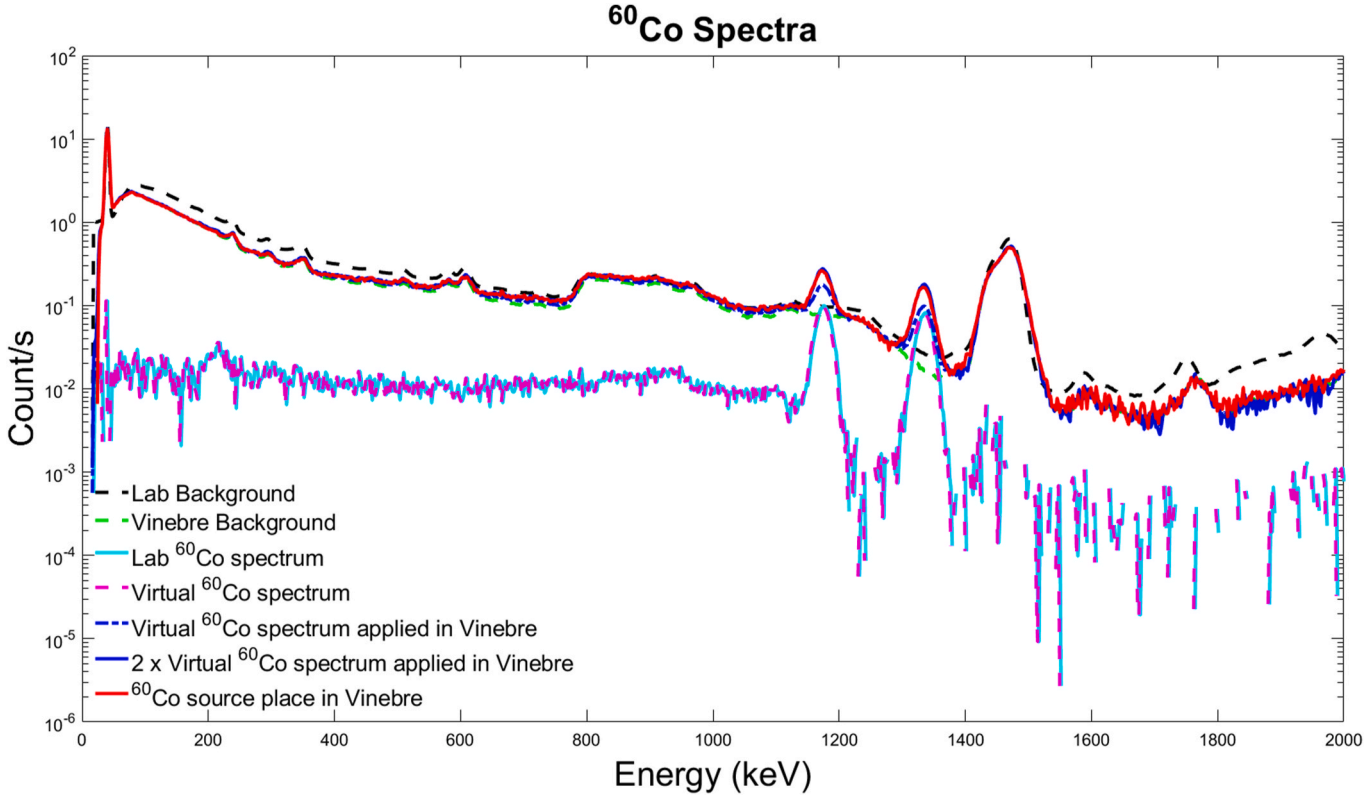

Fig. 16. ^{60}Co spectrum recorded in the laboratory (cyan line) displaced one channel to the left to obtain the ^{60}Co virtual spectrum validated for Vinebre's monitor (dashed magenta line) and applied on Vinebre's monitor (blue dotted line). To obtain the same spectrum as placing a ^{60}Co source next to the Vinebre monitor (red line), it is necessary to multiply by two the virtual spectrum (blue line). The laboratory background spectrum is plotted in the black dashed line and the Vinebre's monitor background is plotted in the green dashed line. For an in-deep image between 1000 and 1800 keV, see Fig. 4.

References

Abida, R., Bocquet, M., Vercauteren, N., Isnard, O., 2008. Design of a monitoring network over France in case of a radiological accidental release. Atmos. Environ. 42, 5205–5219. https://doi.org/10.1016/J.ATMOSENV.2008.02.065.

Alegría, N., Hernández-Ceballos, M.Á., Cinelli, G., Peñalva, I., Muñoz, J.M., 2023. Analysis of 222Rn Surface concentrations in the Basque Country (Spain): a case study of heat waves. Int. J. Environ. Res. Publ. Health 20, 2105. https://doi.org/10.3390/IJERPH20032105, 20, 2105, 2023.

Casanovas, R., Morant, J.J., López, M., Hernández-Girón, I., Batalla, E., Salvadó, M., 2011. Performance of data acceptance criteria over 50 months from an automatic real-time environmental radiation surveillance network. J. Environ. Radioact. 102, 742–748. https://doi.org/10.1016/J.JENVRAD.2011.04.001.

Casanovas, R., Morant, J.J., Salvado, M., 2014a. Development and calibration of a real-time airborne radioactivity monitor using gamma-ray spectrometry on a particulate filter. IEEE Trans. Nucl. Sci. 61, 727–731. https://doi.org/10.1109/TNS.2014.2299715.

Casanovas, R., Morant, J.J., Salvadó, M., 2014b. Development and calibration of a real-time airborne radioactivity monitor using direct gamma-ray spectrometry with two scintillation detectors. Appl. Radiat. Isot. 89, 102–108. https://doi.org/10.1016/J.APRADISO.2014.01.026.

Casanovas, R., Morant, J.J., Salvadó, M., 2013. Implementation of gamma-ray spectrometry in two real-time water monitors using NaI(Tl) scintillation detectors. Appl. Radiat. Isot. 80, 49–55. https://doi.org/10.1016/J.APRADISO.2013.06.003.

Casanovas, R., Morant, J.J., Salvadó, M., 2012a. Temperature peak-shift correction methods for NaI(Tl) and LaBr3(Ce) gamma-ray spectrum stabilisation. Radiat. Meas. 47, 588–595. https://doi.org/10.1016/J.RADMEAS.2012.06.001.

Casanovas, R., Morant, J.J., Salvadó, M., 2012b. Energy and resolution calibration of NaI (Tl) and LaBr3(Ce) scintillators and validation of an EGS5 Monte Carlo user code for efficiency calculations. Nucl. Instrum. Methods Phys. Res. 675, 78–83. https://doi.org/10.1016/J.NIMA.2012.02.006.

Casanovas, R., Prieto, E., Salvadó, M., 2016. Calculation of the ambient dose equivalent H*(10) from gamma-ray spectra obtained with scintillation detectors. Appl. Radiat. Isot. 118, 154–159. https://doi.org/10.1016/J.APRADISO.2016.09.001.

Cerezo, A., Prieto, E., Reichardt, I., Casanovas, R., Salvadó, M., 2023. A fast algorithm for real-time monitoring of artificial radioisotopes in presence of variable natural radioactivity. Radiat. Phys. Chem. 209, 110946 https://doi.org/10.1016/J.RADPHYSCHEM.2023.110946.

Consejo de Seguridad Nuclear, n.d. Suceso de liberación de partículas radiactivas en c.n. ascó i. descripción y consecuencias radiológicas [WWW Document]. URL https://www.csn.es/documents/10182/261583/Suceso+de+liberaci%C3%B3n+de+partículas+radiactivas+en+CN+Asc%C3%B3+I+-+Descripci%C3%B3n+y+consecuencias+radiol%C3%B3gicas (accessed 3.18.24).

Dąbrowski, R., Dombrowski, H., Kessler, P., Röttger, A., Neumaier, S., 2017. Detection of rain events in radiological early warning networks with spectro-dosimetric systems. J. Instrum. 12, P10005 https://doi.org/10.1088/1748-0221/12/10/P10005.

De Felice, P., 2001. The quality assurance programme for the national radioactivity surveillance network in Italy. Radiat Prot Dosimetry 97, 313–316. https://doi.org/10.1093/OXFORDJOURNALS.RPD.A006678.

Hiemstra, P.H., Pebesma, E.J., Twenhöfel, C.J.W., Heuvelink, G.B.M., 2009. Real-time automatic interpolation of ambient gamma dose rates from the Dutch radioactivity monitoring network. Comput. Geosci. 35, 1711–1721. https://doi.org/10.1016/J.CAGEO.2008.10.011.

IAEA, 2018. IAEA Safety Standards for protecting people and the environment. Occupational Radiation Protection.

Iaea, n.d. Naturally Occurring Radioactive Material (NORM VII).

Kessler, P., Behnke, B., Dabrowski, R., Dombrowski, H., Röttger, A., Neumaier, S., 2018. Novel spectrometers for environmental dose rate monitoring. J. Environ. Radioact. 187, 115–121. https://doi.org/10.1016/J.JENVRAD.2018.01.020.

Leontaris, F., Clouvas, A., Xanthos, S., Maltezos, A., Potiriadis, C., Kiriakopoulos, E., Guilhot, J., 2018. Response of the Greek early warning system reuter-Stokes ionization chambers to terrestrial and cosmic radiation evaluated in comparison with spectroscopic data and time series analysis. Radiat Prot Dosimetry 178, 276–287. https://doi.org/10.1093/RPD/NCX107.

Madruga, M.J., 2008. Environmental radioactivity monitoring in Portugal. Appl. Radiat. Isot. 66, 1639–1643. https://doi.org/10.1016/J.APRADISO.2008.04.008.

Mitra, P., Singha Roy, A., Verma, A.K., Pant, A.D., Prakasha, M.S., Anilkumar, S., Vinod Kumar, A., 2016. Application of spectrum shifting methodology to restore NaI(Tl)-recorded gamma spectra, shifted due to temperature variations in the environment. Appl. Radiat. Isot. 107, 133–137. https://doi.org/10.1016/J.APRADISO.2015.10.002.

Neumaier, S., 2017. Final Publishable Report Metrology for Radiological Early Warning Networks in Europe (ENV57)).

Office for Nuclear Regulation, n.d. ONR - FOI release - Detected levels of radioactivity at Sellafield - January 2014 [WWW Document]. URL https://webarchive.nationalarchives.gov.uk/ukgwa/20170106094805/http://www.onr.org.uk/foi/2014/20140020360.htm (accessed 3.19.24).

Ontalba, M.Á., Corbacho, J.Á., Baeza, A., Vasco, J., Caballero, J.M., Valencia, D., Baeza, J.A., 2022. Radiological Alert Network of Extremadura (RAREx) at 2021:30 years of development and current performance of real-time monitoring. Nucl. Eng. Technol. 54, 770–780. https://doi.org/10.1016/J.NET.2021.08.007.

Prieto, E., Casanovas, R., Salvadó, M., 2018a. Spectral windows analysis method for monitoring anthropogenic radionuclides in real-time environmental gamma-ray scintillation spectrometry. J. Radiol. Prot. 38, 229. https://doi.org/10.1088/1361-6498/AA9B9C.

Prieto, E., Casanovas, R., Salvadó, M., 2018b. Calibration and performance of a real-time gamma-ray spectrometry water monitor using a LaBr3(Ce) detector. Radiat. Phys. Chem. 144, 444–450. https://doi.org/10.1016/J.RADPHYSCHEM.2017.10.008.

Sáez-Muñoz, M., Cerezo, A., Prieto, E., Salvadó, M., Vildosola Hernandez, I., Duch, M.A., Camp, A., Gallego, E., Gonzalez-Cadelo, J., Verdú, G., 2024. Recent radiation protection activities related to nuclear facilities on the Iberian Peninsula. Nucl. Eng. Des. 417, 112826 https://doi.org/10.1016/J.NUCENGDES.2023.112826.

Stöhlker, U., Bleher, M., Doll, H., Dombrowski, H., Harms, W., Hellmann, I., Luff, R., Prommer, B., Seifert, S., Weiler, F., 2019. The German dose rate monitoring network and implemented data harmonization techniques. Radiat Prot Dosimetry 183, 405–417. https://doi.org/10.1093/RPD/NCY154.

Štuhec, M., Zorko, B., Mitić, D., Miljanić, S., Ranogajec-Komor, M., 2006. Quality assurance of environmental gamma radiation monitoring in Slovenia. Radiat Prot Dosimetry 121, 191–194. https://doi.org/10.1093/RPD/NCI380.

Toivonen, H., Vesterbacka, K., Pelikan, A., 2008. LaBr3 Spectrometry for Environmental Monitoring.

Unidad de Protección Civil, 2009. PENTA. Plan de Emergencia Nuclear Exterior a las Centrales Nucleares de Ascó y Vandellós.

Union, P.O. of the E., 2000. CELEX1, 2000/473/Euratom: commission recommendation of 8 June 2000 on the application of Article 36 of the Euratom Treaty concerning the monitoring of the levels of radioactivity in the environment for the purpose of assessing the. Exposure of the Population as a Whole (Notified under Document Number C(2000) 1299).